Engineered Science
DOI: https://dx.doi.org/10.30919/es1910

Intelligent Detection of Void Fraction of Annular Two-Phase Flow Regime Using Energy Characteristic Obtained from Image Tomography

Mohammad Reza Emamian,[1] Mohammad Hossein Shahsavari,[1] Seyed Mehdi Alizadeh,[2] Umer Hameed Shah[3,*] and Gholam Hossein Roshani[1,*]

Abstract

This study presents a novel method for accurately measuring the void fraction in annular two-phase air-water flow using a concave 8-blade capacitive sensor, validated through both simulations and experiments. The capacitance values obtained from different electrode configurations were used to generate sinograms. Firstly, tomographic images of the flow were constructed from these matrixes using the back-projection algorithm. Then, the energy of the sinograms was used as the primary input for an Artificial Neural Network (ANN). An optimized Multilayer Perceptron (MLP) network was designed to predict void fractions with high accuracy. Replacing multiple inputs with the energy characteristic greatly enhanced computational efficiency. The method achieved a Mean Absolute Error (MAE) of 0.003 (training) and 0.002 (testing), with R^2 scores of 0.9992 and 0.9997, and Root Mean Square Error (RMSE) of 0.005 (training) and 0.008 (testing), confirming the model's robustness. These results highlight the enhanced sensitivity and precision of the proposed method in void fraction measurement. Moreover, tomographic reconstructions of flow patterns provided valuable insights into the material distribution within the system, contributing to improved process optimization and safety in high-speed fluid environments.

Keywords: Capacitance-based sensors; Artificial intelligence; Void fraction; Sinogram; Image reconstruction.
Received: 11 September 2025; Revised: 15 November 2025; Accepted: 27 November 2025
Article Type: Research article.

1. Introduction

In industries such as chemical, petrochemical, oil, and gas, two-phase flows (*e.g.*, air-oil, water-oil, and air-water mixtures) are commonly encountered.[1] Understanding the gas-liquid flow patterns are crucial for designing and operating industrial systems. However, accurately measuring flow in these mixtures remains challenging.[2] Void fraction is a key parameter for process optimization, safety, quality control, environmental protection, and resource management.[3] Various commercially available meters based on different measurement concepts are currently available to address these challenges.[4,5] Although available, each metering technique has limitations, often depending on flow regime and being accurate only for homogeneous flows; flow-mixing devices are used to improve reliability.[6] Traditional methods that separately measure each fluid phase have proven to be time-consuming and expensive.[7] Therefore, there is a need for a flow meter capable of identifying the flow regime and measuring the void fraction within a pipeline without disrupting ongoing operations.[8,9] A common approach to evaluate the void fraction in gas-liquid flows involves partitioning the gas phase throughout the entire flow volume, allowing for its quantification. Various methods are employed to determine the void fraction, including radiation attenuation, ultrasonic waves, capacitance-based impedance measurements, wire mesh sensors, and valve manipulation.[10–14] Among these, capacitance-based sensors are promising since they measure void fraction without phase separation or process disruption. Electrode arrangement strongly affects accuracy, with concave, ring, or helix types chosen based on fluid properties.

Previous studies have focused on two-phase flows within pipes, such as stratified, annular, and homogeneous

[1]*Electrical Engineering Department, Kermanshah University of Technology, Kermanshah, 6715685420, Iran*
[2]*Petroleum Engineering Department, Australian University, West Mishref, 13015, Kuwait*
[3]*Department of Mechanical Engineering and Artificial Intelligence Research Center, College of Engineering and Information Technology, Ajman University, Ajman, PO Box 346, United Arab Emirates*
[*]*Email:* m.shah@ajman.ac.ae (Umer Hameed Shah), hosseinroshani@kut.ac.ir (Gholam Hossein Roshani)

regimes.[15–18] Abouelwafa and Kendall compared capacitance sensor designs for two-phase pipelines, finding the double helix most practical, while a four-concave-plate design offered better sensitivity in certain flow patterns.[19] Ahmed *et al*. investigated capacitance sensors for measuring void fractions in air-oil two-phase flows, finding that ring-type sensors were more sensitive than concave sensors for detecting void fractions.[20] Tollefsen and Hammer developed a capacitance sensor for measuring the water fraction and undissolved gas in crude oils, using Finite Element Method (FEM) simulations to achieve higher accuracy compared to other non-intrusive sensors.[21] Chen *et al*. (2023) introduced an ANN-based method to measure gas percentages in two-phase flows without recalibration, combining capacitance sensors and COMSOL simulations to achieve high accuracy (MAE = 4.919).[22] Krupa and colleagues developed a concave-shaped capacitive sensor to measure the air fraction in small channels, employing a high-frequency oscillator for gas fraction measurement.[23] Roshani *et al*. conducted experimental research using a capacitive sensor and ANN to measure void fractions in two-phase annular flows for different fluids. They validated their finite element simulations against experimental results for water-air flows and demonstrated high accuracy in predicting void fractions for various liquid-gas mixtures.[24] Shahsavari *et al*. proposed an optimized capacitive sensor with a novel electrode configuration for measuring void fractions in gas-oil two-phase flows. Their simulations using COMSOL Multiphysics showed higher sensitivity compared to traditional sensor designs.[25] Jaworek and Krupa introduced a radio-frequency resonance capacitance sensor for measuring the gas-liquid volume ratio, utilizing semi-cylindrical electrodes to enhance measurement precision.[26] Zhai and colleagues created a concave capacitance sensor system to measure the complex admittance in horizontal oil-water flows, highlighting the influence of flow patterns and excitation frequencies on measurement accuracy.[27] Kendoush and Sarkis improved void fraction measurements by testing different capacitor configurations, reducing statistical error through optimized electrode spacing.[28] Salehi *et al*. introduced a twin rectangular fork-like capacitance sensor (TRFLC) to identify flow regimes in horizontal gas-oil flows. They demonstrated that this design, through FEM simulations, provided better sensitivity compared to concave sensors, particularly for slug flow identification.[29]

In this study, simulations were performed to generate different void fractions in an air-water annular two-phase flow, ranging from fully occupied (0) to completely empty (1). An 8-blade concave capacitive sensor was used. Experiments were conducted to validate the simulations. Using the Finite Element Method (FEM) and COMSOL Multiphysics, capacitance values were measured across various electrode pairs. These capacitance values were then used to construct sinograms, whose energy characteristics served as inputs for a Multilayer Perceptron (MLP) neural network model implemented in MATLAB. The model predicted the void fractions, and sinograms were further utilized for fluid image reconstruction using the back-projection method to enhance understanding.

2. Simulation

The goal of this study was to measure the void fraction in a two-phase air-water flow, specifically focusing on annular flow patterns. In annular gas-liquid flow, the gas and liquid phases remain separated, with gas typically flowing in the center and liquid forming a film along the walls of the pipe. The formation of this flow pattern is influenced by several factors, including fluid properties, pipe diameter, flow velocity, and surface tension between the phases. To simulate and analyze these conditions, COMSOL Multiphysics, a widely recognized software for industrial applications, was used. COMSOL uses the finite element method (FEM) to provide precise simulations across various fields, including mechanical and electronic engineering. In this study, FEM was employed to simulate the electric fields generated by the capacitor plates used in void fraction measurement. As the distance between the electrodes increases, the strength of the electric field decreases, following an inverse cubic relationship with the gap size. A static analysis was applied, as the electric field remained stable over time. COMSOL's FEM-based simulation environment provided various meshing options to ensure accurate results. To improve precision, the mesh resolution was refined, with smaller elements used for detailed calculations. This finer mesh enhanced the accuracy of the simulation, with the mesh dimensions summarized in Table 1.

Table 1: Properties of the Mesh Model.

Feature	Value
Number of vertex elements	88
Number of edge elements	3948

The capacitance (C) of the 8-blade concave sensor is governed by the electric field distribution, which depends on the permittivity of the gas (ε_g) and liquid (ε_l) phases, as well as their spatial arrangement. According to Eq. (1), capacitance is determined by the following relationship:

$$C=\int_V \varepsilon(x,y,z)\cdot E(x,y,z)dV \quad (1)$$

Here, ε(x, y, z) denotes the spatially varying permittivity, E(x, y, z) represents the electric field intensity, and V refers to the sensing volume. In annular flow conditions, the presence of a gas core surrounded by a liquid film induces radial variations in ε(x, y, z), necessitating numerical analysis for precise characterization. To explore this phenomenon, simulations were conducted using boundary conditions that account for the concave geometry of the electrodes and the dielectric interface between the gas and liquid phases. As described by Eq. (2),[30] the electric field E between the electrodes follows Laplace's equation:

$$\nabla^2\varphi=0 \quad (2)$$

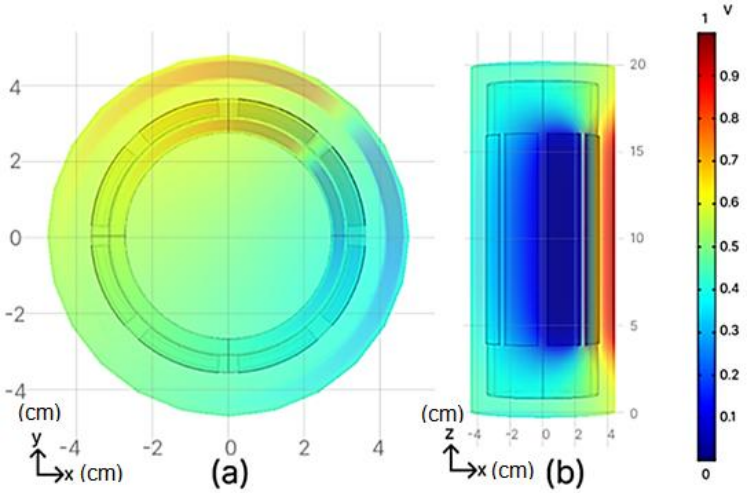

Fig. 1: Surface plots of electric potential distribution in the sensing domain of the 8-blade concave capacitive sensor under annular flow conditions: (a) in the xy-plane and (b) in the yz-plane, highlighting field intensity across the cross-section.

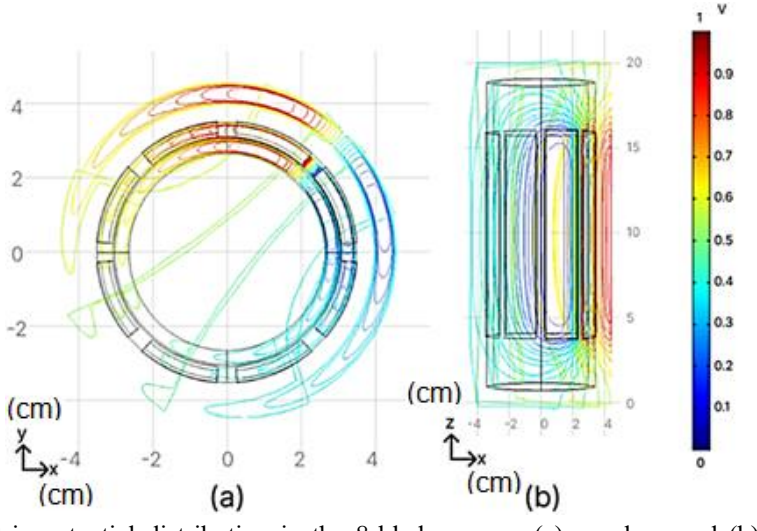

Fig. 2: Contour plots of electric potential distribution in the 8-blade sensor: (a) xy-plane and (b) yz-plane, illustrating spatial variations in the electric field, especially near electrode boundaries where sensitivity is highest.

The symbol φ denotes the electric potential. Fig. 1(a) displays a surface plot of the potential distribution in the xy-plane, highlighting its behavior within the annular flow regime. Fig. 1(b) shows the corresponding surface plot in the yz-plane, offering a detailed view of field variations. Similarly, Fig. 2(a) presents a contour plot of the field distribution along the sensor length in the xy-plane, while Fig. 2(b) illustrates the corresponding contour plot in the yz-plane.

Edge effects can significantly influence the electric field distribution and capacitance measurements, especially when the liquid film thickness is thin. To address this, a "finer" mesh was utilized in the COMSOL simulations, particularly near the electrode edges, to accurately capture these effects. The results, shown in Fig. 1 and Fig. 2, demonstrate that the edge effects follow a predictable pattern, as described by Eq. (3):

$$\Delta C \propto \frac{1}{d^3} \tag{3}$$

where d represents the electrode spacing. This relationship ensures that the edge effects remain within acceptable limits for the sensor configuration.

Additionally, the concave geometry of the electrodes is specifically designed to effectively manage the electric field distribution, particularly within the annular regime. As shown in the contour plots of Fig. 2(a) and Fig. 2(b), field uniformity is maintained across the entire region, including the edges. This demonstrates the successful measurement of the electric field through the designed geometry. The computational analysis was performed on a system equipped with an Intel 11th-generation i5 processor and 12 GB of RAM. While the computational setup was sufficient for the task, the finer mesh resolution increased the demand for processing power and memory, resulting in more detailed and accurate simulations of the void fraction. Each FEM simulation conducted in COMSOL Multiphysics required approximately 30 seconds to complete, with an additional 10 seconds needed to update parameters between runs. To optimize computational efficiency, we employed the parametric sweep functionality in COMSOL. This approach enabled automatic variation of input

parameters such as void fraction, significantly reducing manual workload and total simulation time across all 336 runs. Furthermore, to ensure accurate representation of the electric field, particularly in regions near electrode edges where field intensities change rapidly, we utilized a finer meshing strategy. This mesh refinement improved the precision of the capacitance measurements while maintaining acceptable computational times. The balance between mesh resolution and computational speed was carefully managed to ensure both accuracy and efficiency throughout the study.

2.1 Validation

Annular flow is characterized by a thin liquid layer flowing along the pipe walls, while the gas phase moves through the central region. The schematic representation of an annular regime is illustrated in Fig. 3. The volume fraction in this water–gas two-phase flow regime was determined using Eq. (4) and (5).

$$V_{Air} = \frac{\pi r_2^2}{\pi r_1^2} = \frac{r_2^2}{r_1^2} \quad (4)$$

$$V_{Liquid} = \frac{\pi r_1^2 - \pi r_2^2}{\pi r_1^2} = \frac{r_1^2 - r_2^2}{r_1^2} \quad (5)$$

Due to the challenges associated with replicating annular flow in a laboratory setting, a static experimental setup was implemented. To achieve phase separation, thin PVC films were used to fabricate models with varying diameters. However, these separator pipes were excluded from the simulations due to their minimal thickness. A 3D-printed PLA pipe with a relative permittivity of 3.3 was utilized for the experiments. The pipe was constructed using transparent filament and had the following dimensions: a length of 18 cm, an inner radius of 28 mm, and an outer radius of 32 mm.

Electrodes were fabricated by cutting a thin copper sheet into eight concave-shaped segments, each with a length of 12 cm and spaced 5 mm apart. Capacitance measurements were conducted across a range of void fractions (0, 0.05, 0.1, 0.15, 0.2, 0.25, 0.3, 0.35, 0.4, 0.45, 0.5, 0.55, 0.6, 0.65, 0.7, 0.75, 0.8, 0.85, 0.9, 0.95, and 1). To validate the results, experimental capacitance values were compared with numerical simulations, and the experimental setup was documented accordingly. As depicted in Fig. S1, the system was designed to measure capacitance for various electrode configurations. Since the study focuses on annular flow, capacitance measurements from both adjacent and opposite electrode pairs were considered representative of the overall behavior.

A total of 21 capacitance measurements were performed for each electrode pair, covering different void fraction levels. Additionally, the same electrode configurations were simulated using COMSOL Multiphysics. Fig. 4 illustrates a comparative analysis of experimental and simulated

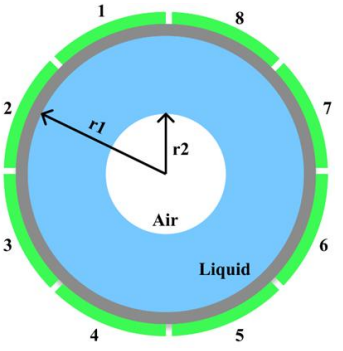

Fig. 3: Schematic of the annular gas-liquid two-phase flow regime, showing the 8 concave electrodes arranged around the pipe for capacitance-based void fraction measurement.

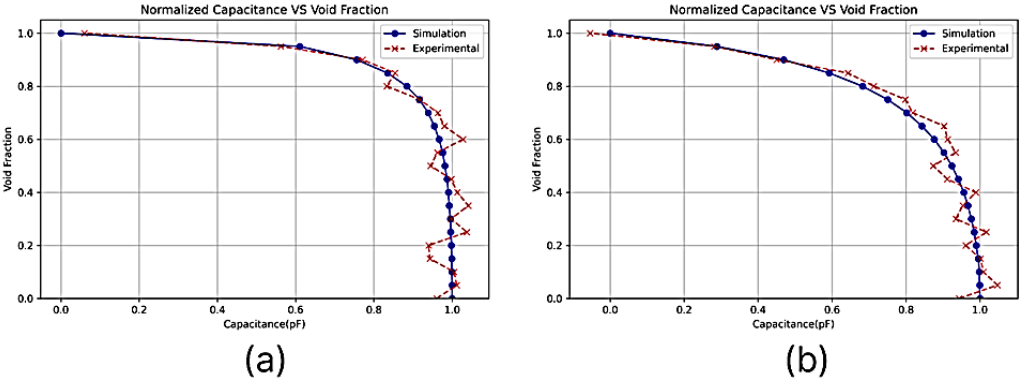

Fig. 4: A comparative analysis of experimental and simulated capacitance values for (a) Electrodes No. 1 and 2 (b) Electrodes No. 8 and 3.

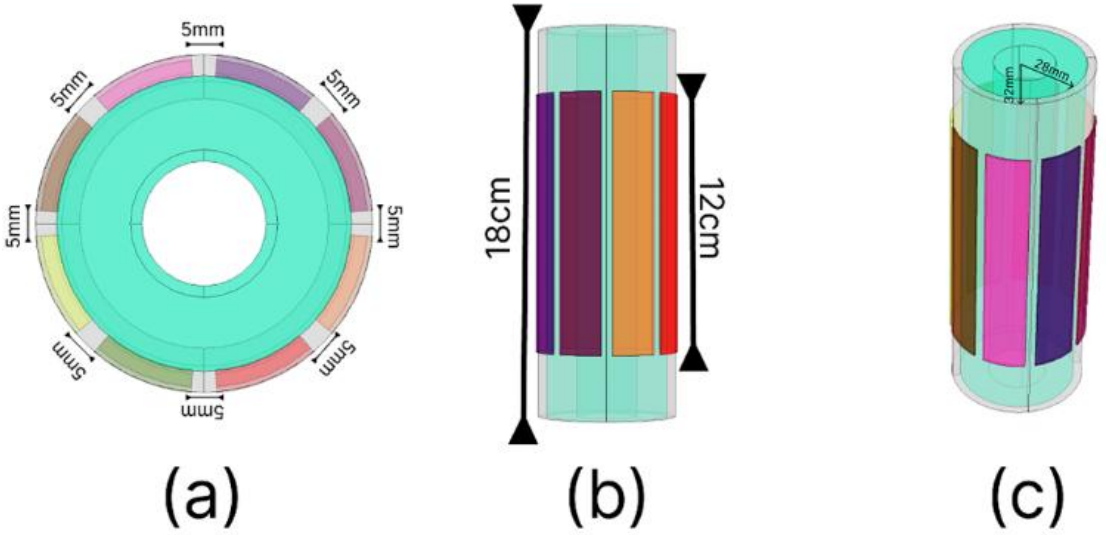

Fig. 5: Geometric model of the 8-blade sensor and pipeline showing electrode placement for simulation and measurement: (a) xy-plane view, (b) xz-plane view, and (c) custom 3D view.

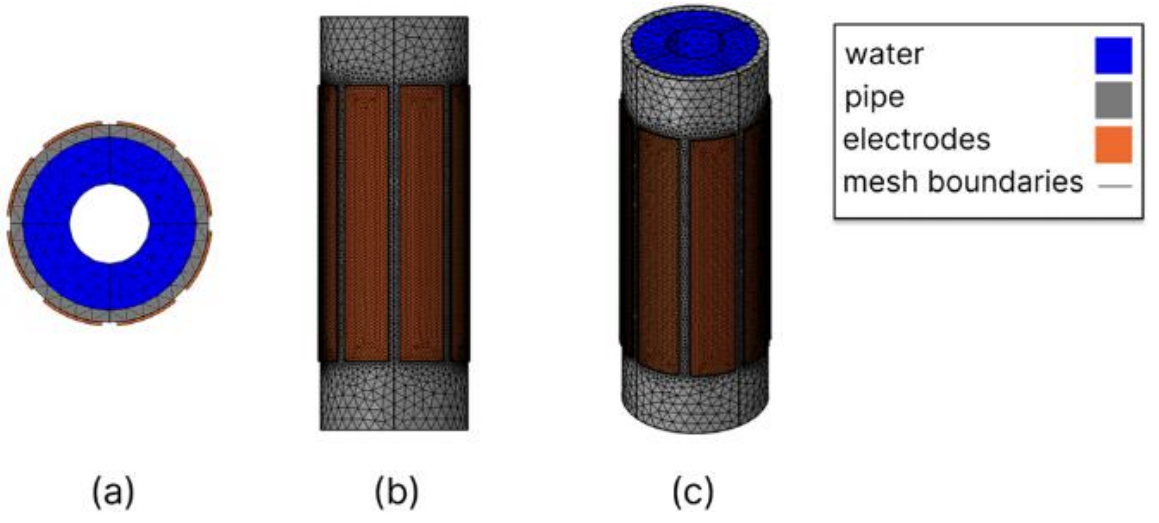

Fig. 6: Finite element mesh of the 8-blade concave sensor in (a) xy-plane, (b) xz-plane, and (c) 3D view, using a finer mesh to ensure high accuracy near electrode edges where electric field gradients are most significant.

capacitance values for selected electrode pairs.

2.2 Sensor geometry and analyses

The 8-blade concave sensor was modeled and simulated using COMSOL Multiphysics. The schematic representation of the pipe is shown in both the xy plane (Fig. 5(a)) and the xz plane (Fig. 5(b)), with a custom view provided in Fig. 5(c). For the simulation, a high precision setting was used, and the geometry was subdivided into 509,580 domain elements for detailed analysis. The meshed model is illustrated in Fig. 6, with views in the xy plane (Fig. 6(a)) and the xz plane (Fig. 6(b)), along with a custom view in Fig. 6(c).

The main aim of this research is to evaluate the void fraction through the sinogram matrix energy while generating a tomographic representation of fluid flow to enhance user comprehension. Tomography primarily focuses on understanding the distribution of materials within a pipe. This technique, widely acknowledged in the medical field, generally involves two key stages: forward projection and back projection. A variety of methods can be employed for projection, including gamma and X-ray attenuation, sonar-based techniques, and even electrical resistance measurements, among others. All these techniques contribute to the formation of the sinogram image. For the purpose of image reconstruction, several mathematical algorithms such as ART, SART, BP, and FBP are applied. The back projection method is particularly favored for creating tomographic images due to its simplicity in computation, facilitating real-time processing. To achieve this, capacitance measurements are taken across various configurations to execute forward projections and produce the sinogram. Essentially, the sinogram consists of the capacitance values recorded for various pairs of electrodes. It is evident that in this flow regime, all adjacent pairs of electrodes exhibit equal capacitance, while the capacitance values of directly opposing electrodes are also identical. Capacitance measurements are taken at four angles: 0°, 45°,

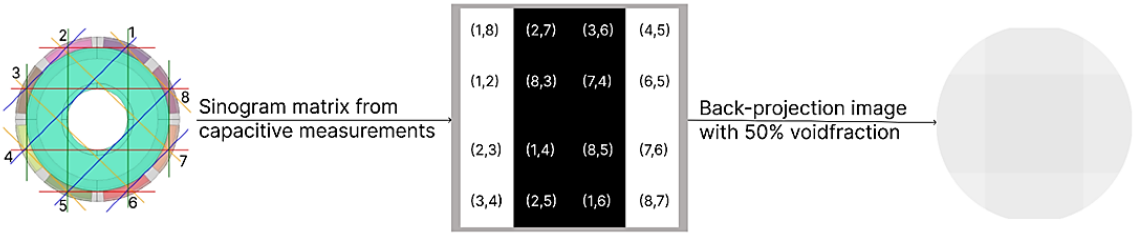

Fig 7: Sinogram generation from capacitance measurements at multiple angles and the corresponding tomographic image showing fluid distribution inside the pipe for a void fraction of 0.5.

90°, and 135°. Following these measurements, the sinogram matrix is constructed. The final image is then created using the back projection method. Fig. 7 depicts the sinogram for a value of 0.5. The angles used in this study (0°, 45°, 90°, and 135°) correspond to the orientation of each pair of opposing electrodes relative to the vertical axis. These four projection angles were selected based on the physical layout of the 8-blade concave sensor, ensuring symmetrical and meaningful coverage of the sensing domain. Each angle effectively captures a distinct cross-sectional view of the material distribution within the pipe. While the current configuration provides satisfactory image reconstruction and prediction accuracy, increasing the number of projection angles would indeed improve the resolution and detail of the reconstructed tomographic images. This is because more projection angles lead to a denser sinogram, which increases the number of sinogram pixels and subsequently enhances the granularity of the generated image. Achieving this would require either increasing the number of electrodes or reconfiguring the measurement strategy. Although this study prioritizes computational simplicity, future research could explore the use of higher angular resolution to further improve the fidelity of the reconstructed images and potentially extract more detailed features from the flow. (Fig. 7).

3. Computational methods

The main novelty of this study lies in its ability to determine the void fraction with significantly improved accuracy compared to previous works by incorporating ANN and the energy derived from the pipe's sinogram matrix. Nowadays AI is widely used as solution for many different scenarios that is why we can see its trace in many fields ranging from health and civil to generating images.[31-33] The sinogram matrix, which represents the distribution of capacitance values obtained from a capacitive sensing system, is used to analyze the void fraction in a two-phase flow. This matrix reflects how the material is distributed across the sensing area. Instead of using 16 individual pixel inputs, these were transformed into a single input - the sinogram energy matrix - using Eq. (6). By employing this energy matrix, the ANN model can more effectively analyze the void fraction within the flow.

$$E=\sum_{i=1}^{m}\sum_{j=1}^{n}\left|M_{ij}\right|^{2} \qquad (6)$$

where M(i,j) represents the sinogram matrix element, m is the number of rows, and n is the number of columns. By consolidating the spatial information into a single metric, computational complexity is significantly reduced without sacrificing prediction accuracy. The results clearly demonstrate that the energy feature contributes to achieving high prediction accuracy, significantly reducing model error. Both the training and testing data have shown highly satisfactory accuracy levels, leading to a substantial improvement in the model's performance in detecting two-phase flow patterns.

To systematically optimize the MLP architecture, an extensive hyperparameter search was performed by varying key model parameters. Specifically, the number of hidden layers was explored within the range of 1 to 5, and the number of neurons per layer was set between 3 and 10. The training process was evaluated using epoch counts from 100 to 700, and four different learning rates (0.001, 0.005, 0.01, and 0.05) were compared. The optimal configuration was determined by evaluating both model performance and computational cost, resulting in a single hidden layer with seven neurons, a learning rate of 0.01, and 500 epochs. This setup consistently exhibited the lowest error rates and superior convergence behavior during all training trials.

To evaluate model performance, the Mean Squared Error (MSE) criterion was used, as shown in Eq. (7):

$$E=\frac{1}{N}\sum_{i=1}^{N}\left(y_i^{predicted}-y_i^{actual}\right)^{2} \qquad (7)$$

where N represents the number of data points, $y_i^{predicted}$ is the predicted output from the MLP, and y_i^{actual} is the actual ground truth value. This method allowed for systematic refinement of neurons and epochs, ensuring stability and accuracy in the final configuration. For illustration of the optimization process, the "Loss vs Epoch" plot was provided in Fig. 8. This plot demonstrates how the model's loss decreased over the course of training epochs, achieving convergence after a certain number of iterations. This graphical representation further emphasizes the stability and consistency of the model's performance. The optimization process of the MLP model was illustrated in Fig. 9

To enhance the optimization process, key hyperparameters were systematically adjusted. The learning rate (η) was set to

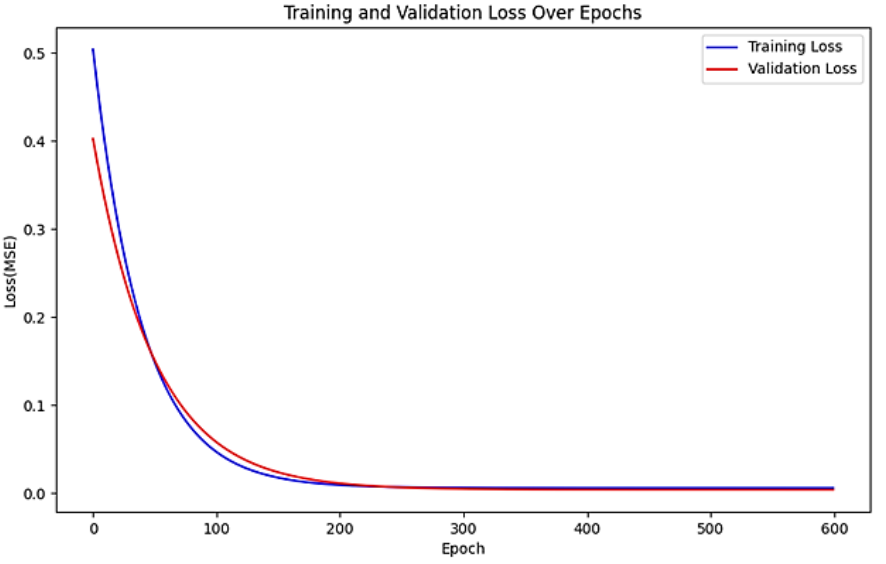

Fig. 8: Loss vs Epoch plot demonstrating convergence during MLP training.

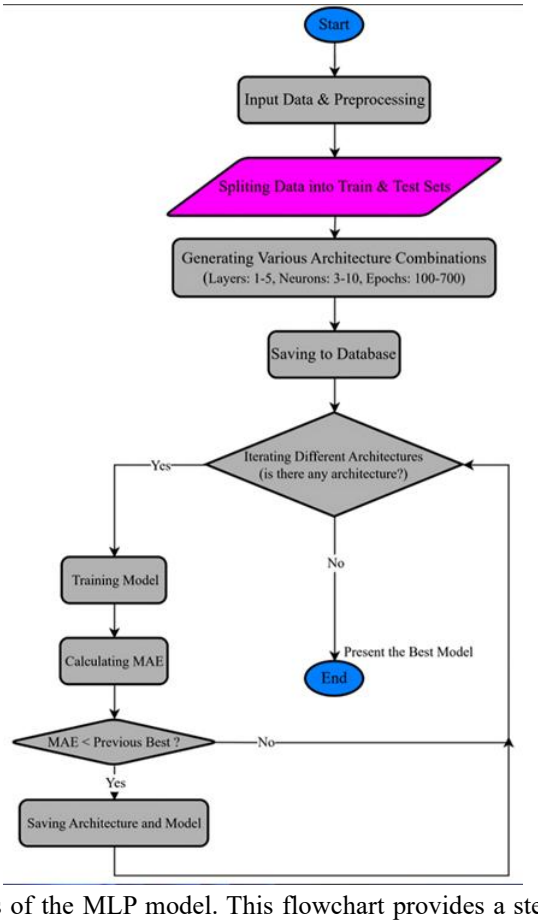

Fig. 9: Illustrates the optimization process of the MLP model. This flowchart provides a step-by-step visual representation of the entire process, from data preprocessing to model training and the final model selection.

0.01 to balance convergence speed and stability. The weight update rule during backpropagation follows Eq. (8):

$$w_{new}=wold_{old}-\eta\cdot\frac{\partial E}{\partial w} \quad (8)$$

where w_{new} represents the updated weight, $wold_{old}$ is the previous weight, η is the learning rate ($\eta = 0.01$), and $\frac{\partial E}{\partial w}$ denotes the gradient of the error function E. These adjustments ensured that training progressed efficiently while preventing instability due to overly aggressive updates.

Although advanced architectures such as Convolutional Neural Networks (CNNs) offer benefits in certain applications, the focus of this study was to demonstrate the effectiveness of a simpler MLP model for void fraction prediction. The high

accuracy achieved highlights the suitability of MLP without necessitating computationally expensive alternatives. From a theoretical perspective, computational complexity was considered when comparing MLP with CNN. Due to its simpler structure, MLP is particularly well-suited for processing data with limited features, such as a sinogram energy matrix. It primarily relies on weighting and aggregating inputs at network layers, requiring significantly fewer computations compared to CNN, which involves complex convolutional operations and multi-step processing. These additional computational demands make CNNs more suited for large-scale image analysis, whereas the structured input data in this study did not necessitate such complexity. As a result, MLP efficiently minimized computational costs while maintaining high predictive accuracy.

The choice of the Multilayer Perceptron (MLP) model in this study was deliberate and based on the nature of the input data and computational efficiency requirements. The sinogram energy metric used as input is a compact, one-dimensional feature that summarizes the overall spatial distribution within the tomographic data. Given the low dimensionality and structured nature of the input, MLP provides a fast, stable, and computationally lightweight model capable of achieving high accuracy without the complexity of more advanced architectures. Unlike Convolutional Neural Networks (CNNs), which are ideal for high-dimensional and spatially rich input such as images, or transformer-based models, which require significant training data and processing power, MLP offered a pragmatic solution aligned with our study's goals. However, we recognize the strengths of these modern AI architectures and suggest that future studies could explore CNNs or transformer-based models, particularly if full sinogram matrices or reconstructed images are to be used directly as inputs. Such exploration may offer additional improvements in predictive performance, especially for more complex flow regimes or real-time monitoring applications.

The hidden layer utilized the tansig activation function, which maps inputs to the range [-1, 1]. This function is particularly effective for normalized data like the sinogram energy matrix and contributes to stable training dynamics. Mathematically, it is expressed as shown in Eq. (9):

$$f(x)=\frac{2}{1+e^{-2x}}-1 \tag{9}$$

This activation function played a crucial role in maintaining numerical stability and enhancing learning efficiency. By employing MLP with carefully tuned hyperparameters and an appropriate activation function, a computationally efficient yet highly accurate model was developed, significantly improving void fraction prediction while minimizing processing costs.

Using the COMSOL Multiphysics software, a total of 336 simulations were carried out, where void fractions were varied in steps of 5% from 0 to 100. Out of these simulations,70% were designated for training the network, while the remaining 30% were set aside for testing purposes. The specific details

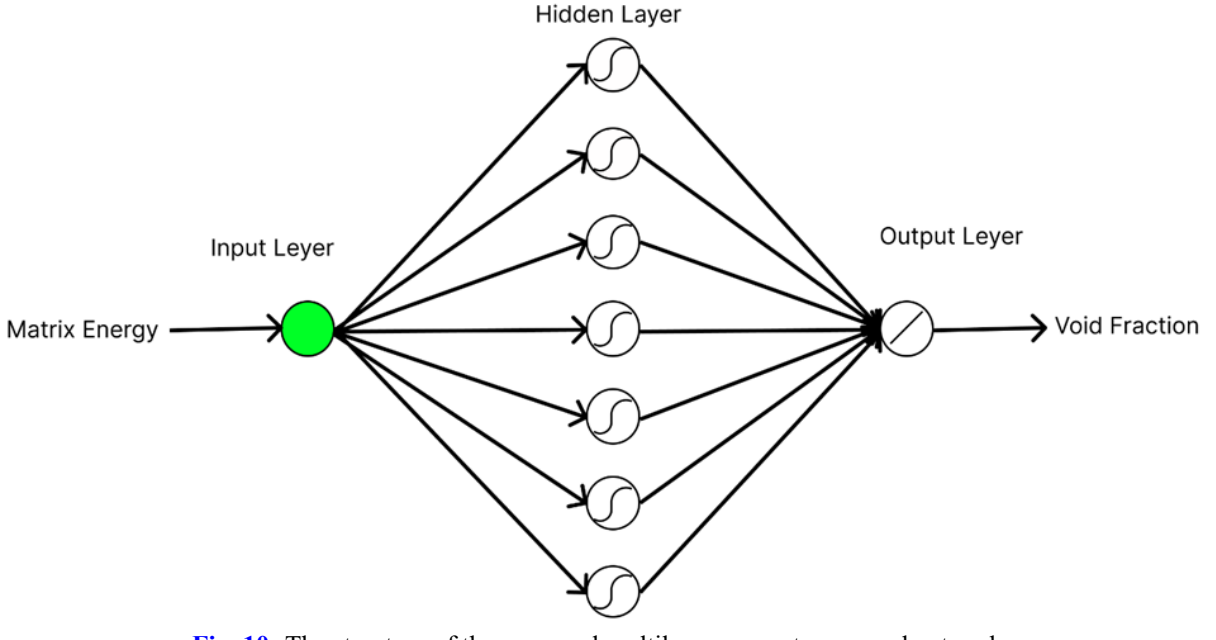

Fig. 10: The structure of the proposed multilayer perceptron neural network.

Table 2: Features of the suggested ANN.

Type of network	MLP
Number of inputs	1
Input and output layers activation function	Purelin

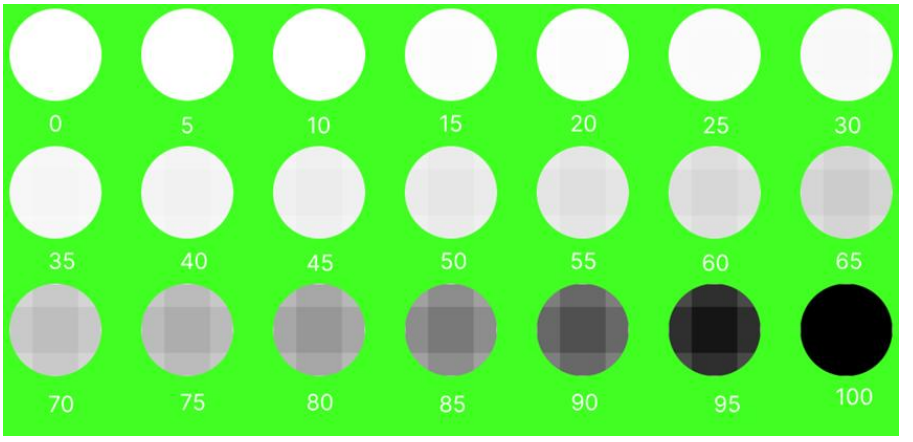

Fig. 11: Reconstructed visuals of various void fraction values.

of this model configuration are provided in Fig. 10 and Table 2. Fig. 11 illustrates the pipe tomography along with various void fraction levels.

4. Results and discussion

Measuring the void fraction is essential for optimizing processes, ensuring safety, maintaining product quality, minimizing environmental risks, efficiently utilizing resources, and advancing scientific knowledge. Accurate void fraction measurement plays a critical role across various industries, contributing to better performance, reliability, and environmental sustainability. This paper uses a concave 8-blade sensor to measure capacitance values. The Finite Element Method (FEM) was employed through COMSOL Multiphysics to simulate 21 void fractions for annular flow regimes with different electrode configurations. The measured data was then used to generate the necessary sinogram. The main innovation of this research lies in the substantial improvement in the accuracy of void fraction measurement. This enhancement was achieved through a novel approach that leverages the energy matrix of the fluid sinogram along with a neural network. The concave design of the 8-blade sensor provides higher sensitivity compared to sensors with more blades, making it well-suited for high-velocity fluid environments. Furthermore, the sensor's lower computational power requirements boost its overall efficiency. In addition, a tomographic image has been generated to offer users a clearer understanding of flow patterns and material distribution within the system. The results demonstrate that this new method offers high accuracy. The mean absolute error (MAE) of the model, as shown in Eq. (10), is 0.003 for the training set and 0.002 for the testing set. In this equation (N) represents the number of data points, X(pred) refers to the predictions made by the proposed Multi-Layer Perceptron (MLP) model, and X(sim) corresponds to the simulation results obtained from COMSOL.

$$MAE=\frac{1}{N}\sum_{i=1}^{z}|x_i(Sim)-x_i(Pred)| \quad (10)$$

The R^2 score, which indicates the proportion of variance in the dependent variable that is predictable from the independent variables, is calculated using Eq. (11). In this equation, y_i represents the observed values, $\hat{y}_i$ represents the predicted values, $\bar{y}$ is the mean of the observed values, and n is the total number of data points.

$$R^2=1-\frac{\sum_{i=1}^{n}(y_i-\hat{y}_i)^2}{\sum_{i=1}^{n}(y_i-\bar{y})^2} \quad (11)$$

For the training data, the R^2 score is 0.9992, and for the testing data, it is 0.9997. Similarly, the Root Mean Squared Error (RMSE), which measures the average magnitude of the error between observed and predicted values, is calculated using Eq. (12). Here, y_i and $\hat{y}_i$ represent the observed and predicted values, respectively, and n is the total number of data points.

$$RMSE=\sqrt{\frac{1}{n}\sum_{i=1}^{n}(y_i-\hat{y}_i)^2} \quad (12)$$

The RMSE for the training data is 0.005, and for the testing data, it is 0.008. With the high R^2 score, low RMSE values, and low MAE, this model demonstrates excellent predictive accuracy.

Fig. 12 illustrates the regression results for both the training and testing datasets. It is clear that the model does not suffer from underfitting or overfitting. Additionally, the sinogram is utilized to reconstruct the flow pattern and gather insights into the material distribution within the pipe, helping to better understand the internal flow dynamics. This achievement was made possible through a unique approach that combines the energy matrix of the fluid sinogram with a neural network. The decision to use the concave 8-blade sensor, rather than a sensor with more blades, was driven by its larger cross-sectional area, which enhances signal-to-noise ratio while minimizing flow velocity errors. This makes it especially well-suited for high-speed fluid environments. Furthermore, the sensor's lower computational requirements enhance its overall efficiency. To further improve user insights, a tomographic image was also generated. The comparison presented in Table 3, highlights the advancements achieved in

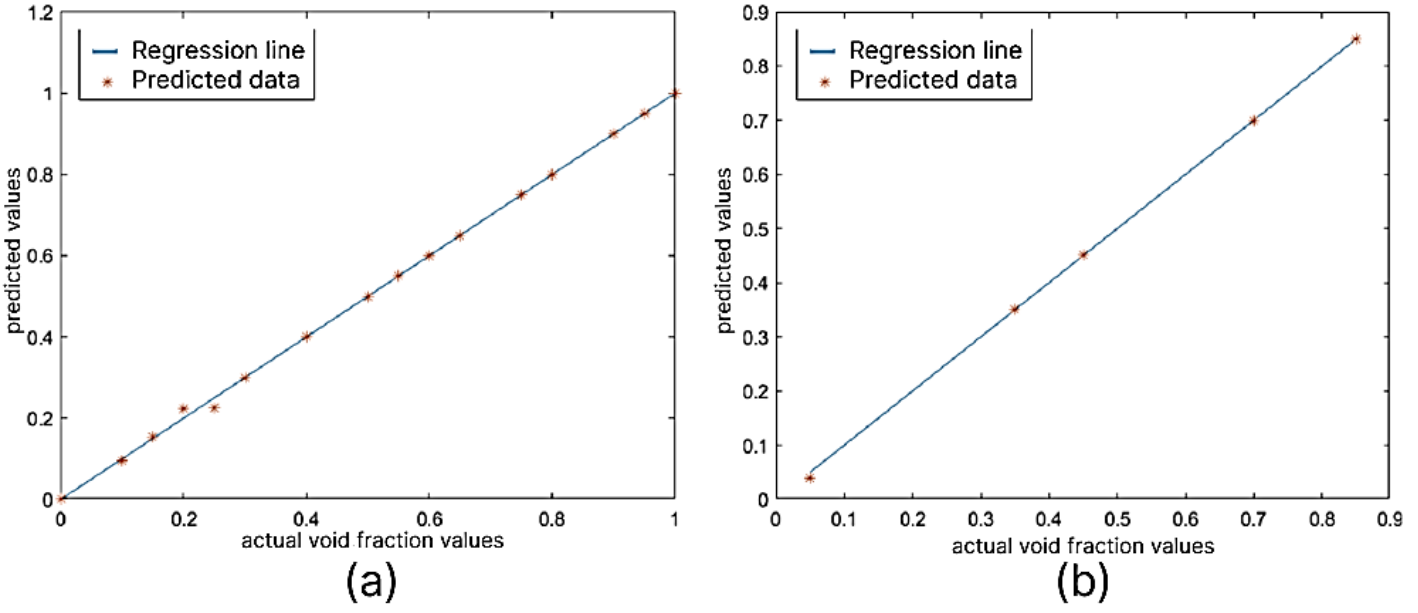

Fig. 12: The regression diagrams for training(a) and testing(b) datasets.

Table 3: Comparison of void fraction measurement studies.

Study	Measurement Technique	Fluids Tested	Reported Accuracy	Achievement
Abouelwafa & Kendall (1980)[19]	Double helix capacitance sensor	Air-oil	Higher linearity than other designs	Demonstrated linearity in measuring void fractions.
Ahmed *et al.* (2006)[20]	Ring-type capacitance sensor	Air-oil	Higher sensitivity than concave sensors	Enhanced sensitivity for air-oil flow measurements.
Salehi *et al.* (2017)[29]	Twin rectangular fork-like capacitance sensor (TRFLC)	Gas-oil	Better sensitivity for slug flow regimes	Improved performance for slug flow detection.
Roshani *et al.* (2023)[24]	Capacitive sensor with ANN	Air-water	High accuracy, validated experimentally	Achieved high accuracy using ANN for experimental data.
Chen *et al.* (2023)[22]	Capacitance-based sensor with ANN	Various liquids	MAE: 4.919	Developed a recalibration-free approach for multiple liquids.
Current Study	8-blade concave capacitive sensor integrated with ANN	Air-water	MAE: 0.003 (training), 0.002 (testing)	Presented tomographic imaging and achieved high precision.

void fraction measurement techniques. While earlier studies employed various capacitance-based sensors and ANNs with moderate accuracy, the proposed method demonstrates a significant improvement in precision. By integrating an 8-blade concave capacitive sensor with an ANN, this study achieved the lowest reported mean absolute error (MAE) of 0.003 for training and 0.002 for testing in air-water flows. Table 3 presents similar studies along with their main achievements. However, the key novelty of the present work lies in employing a different approach for void fraction measurement through tomographic imaging of the pipe. This method achieves a lower MAE compared to the most recent study listed in Table 3, demonstrating a significant improvement over previous works. This marks a substantial enhancement over previous approaches, showcasing the reliability and computational efficiency of the proposed technique for high-accuracy void fraction measurement.

5. Conclusion

This study presents an innovative method for accurately measuring void fractions in annular air-water two-phase flows using an 8-blade concave capacitive sensor. The Finite Element Method (FEM) and COMSOL Multiphysics were employed to simulate various void fractions, with results validated through laboratory experiments. The concave sensor design improved sensitivity in high-velocity flows, while computational efficiency was achieved by using a sinogram-based energy feature with a Multi-Layer Perceptron (MLP) model. This approach achieved a MAE of 0.003 (training) and 0.002 (testing), with R^2 scores of 0.9992 and 0.9997, and RMSE values of 0.005 and 0.008, respectively. The tomographic reconstruction further provided valuable insights into flow patterns, supporting system optimization and safety improvements. This method offers a significant advancement in void fraction measurement with broad industrial applications.

Acknowledgments
This work was supported by Ajman University Internal Research Grant (Grant No.: 2023-IRG-ENIT-38). The research findings presented in this article are solely the author(s) responsibility.

Conflict of Interest
The authors declare no conflict of interest.

Supporting Information
Applicable.

CRediT Statement
Mohammad Reza Emamian: Investigation, Data curation, Software, Formal analysis, Visualization, Writing. **Mohammad Hossein Shahsavari:** Methodology, Software, Validation, Formal analysis, Writing. **Seyed Mehdi Alizadeh:** Conceptualization, Methodology, Resources, Review and editing. **Umer Hameed Shah:** Supervision, Project administration, Validation, Review and editing. **Gholam Hossein Roshani:** Supervision, Conceptualization, Project administration, Review and editing.

References
[1] H. Karimi, M. Boostani, Heat transfer measurements for oil–water flow of different flow patterns in a horizontal pipe, *Experimental Thermal and Fluid Science*, 2016, **75**, 35-42, doi: 10.1016/j.expthermflusci.2016.01.007.
[2] G. Huang, H. Ji, Z. Huang, B. Wang, H. Li, Flow regime identification of mini-pipe gas-liquid two-phase flow based on textural feature series, *IEEE International Instrumentation and Measurement Technology Conference*, Hangzhou, China, May 10-12, 2011, 1-4, doi: 10.1109/IMTC.2011.5944218.
[3] U. Khan, W. Pao, N. Sallih, Numerical gas–liquid two-phase flow regime identification in a horizontal pipe using dynamic pressure data, *Applied Sciences*, 2023, **13**, 1225, doi: 10.3390/app13021225.
[4] T. S. Whitaker, Multiphase flow measurement: current and future developments, *IEE Colloquium on Advances in Sensors for Fluid Flow Measurement*, London, UK, 1996, 1-1, doi: 10.1049/ic:19960569.
[5] R. Thorn, G. A. Johansen, E. A. Hammer, Recent developments in three-phase flow measurement, *Measurement Science and Technology*, 1997, **8**, 691-701, doi: 10.1088/0957-0233/8/7/001.
[6] I. Ismail, J. C. Gamio, S. F. A. Bukhari, W. Q. Yang, Tomography for multi-phase flow measurement in the oil industry, *Flow Measurement and Instrumentation*, 2005, **16**, 145-155, doi: 10.1016/j.flowmeasinst.2005.02.017.
[7] D. Wang, F.-C. Liang, Z.-Q. Peng, Y.-G. Wang, Z.-H. Lin, Gas–liquid two-phase flow measurements by full stream batch sampling, *International Journal of Multiphase Flow*, 2012, **40**, 113-125, doi: 10.1016/j.ijmultiphaseflow.2011.11.010.
[8] M. Banowski, M. Beyer, L. Szalinski, D. Lucas, U. Hampel, Comparative study of ultrafast X-ray tomography and wire-mesh sensors for vertical gas–liquid pipe flows, *Flow Measurement and Instrumentation*, 2017, **53**, 95-106, doi: 10.1016/j.flowmeasinst.2016.02.001.
[9] C. M. Salgado, R. S. F. Dam, E. J. A. Puertas, W. L. Salgado, Calculation of volume fractions regardless scale deposition in the oil industry pipelines using feed-forward multilayer perceptron artificial neural network and MCNP6 code, *Applied Radiation and Isotopes*, 2022, **185**, 110215, doi: 10.1016/j.apradiso.2022.110215.
[10] A. M. Iliyasu, D. K. Bagaudinovna, A. S. Salama, G. H. Roshani, K. Hirota, A methodology for analysis and prediction of volume fraction of two-phase flow using particle swarm optimization and group method of data handling neural network, *Mathematics*, 2023, **11**, 916, doi: 10.3390/math11040916.
[11] S. Al-lababidi, A. Addali, H. Yeung, D. Mba, F. Khan, Gas void fraction measurement in two-phase gas/liquid slug flow using acoustic emission technology, *Journal of Vibration and Acoustics*, 2009, **131**, 064501, doi: 10.1115/1.4000463.
[12] C. G. Xie, A. L. Stott, A. Plaskowski, M. S. Beck, Design of capacitance electrodes for concentration measurement of two-phase flow, *Measurement Science and Technology*, 1990, **1**, 65-78, doi: 10.1088/0957-0233/1/1/012.
[13] M. Abdulkadir, V. Hernandez-Perez, I. S. Lowndes, B. J. Azzopardi, E. T. Brantson, Detailed analysis of phase distributions in a vertical riser using wire mesh sensor (WMS), *Experimental Thermal and Fluid Science*, 2014, **59**, 32-42, doi: 10.1016/j.expthermflusci.2014.07.010.
[14] S. Koyama, J. Lee, R. Yonemoto, An investigation on void fraction of vapor–liquid two-phase flow for smooth and microfin tubes with R134a at adiabatic condition, *International Journal of Multiphase Flow*, 2004, **30**, 291-310, doi: 10.1016/j.ijmultiphaseflow.2003.10.009.
[15] M. H. Shahsavari, A. Veisi, G. H. Roshani, E. Eftekhari-Zadeh, E. Nazemi, An experimental and simulation study for comparison of the sensitivity of different non-destructive capacitive sensors in a stratified two-phase flow regime, *Electronics*, 2023, **12**, 1284, doi: 10.3390/electronics12061284.
[16] D. Strazza, M. Demori, V. Ferrari, P. Poesio, Capacitance sensor for hold-up measurement in high-viscous-oil/conductive-water core-annular flows, *Flow Measurement and Instrumentation*, 2011, **22**, 360-369, doi: 10.1016/j.flowmeasinst.2011.04.008.
[17] A. Zhao, N. Jin, L. Zhai, Z. Gao, Liquid holdup measurement in horizontal oil–water two-phase flow by using concave capacitance sensor, *Measurement*, 2014, **49**, 153-163, doi: 10.1016/j.measurement.2013.11.036.
[18] Ortiz, J.; Masek, V. Cyclonic capacitive sensor for multiphase composition measurement, *Sensors & Transducers*, 2015, **191**, 1–11.
[19] M. S. A. Abouelwafa, E. J. M. Kendall, The use of capacitance sensors for phase percentage determination in multiphase pipelines, *IEEE Transactions on Instrumentation and Measurement*, 1980, **29**, 24-27, doi: 10.1109/TIM.1980.4314856.
[20] H. Ahmed, Capacitance sensors for void-fraction measurements and flow-pattern identification in air–oil two-

phase flow, *IEEE Sensors Journal*, 2006, **6**, 1153-1163, doi: 10.1109/JSEN.2006.881390.
[21] J. Tollefsen, E. A. Hammer, Capacitance sensor design for reducing errors in phase concentration measurements, *Flow Measurement and Instrumentation*, 1998, **9**, 25-32, doi: 10.1016/s0955-5986(98)00006-5.
[22] T.-C. Chen, S. M. Alizadeh, A. K. Alanazi, J. W. Grimaldo Guerrero, H. M. Abo-Dief, E. Eftekhari-Zadeh, F. Fouladinia, Using ANN and combined capacitive sensors to predict the void fraction for a two-phase homogeneous fluid independent of the liquid phase type, *Processes*, 2023, **11**, 940, doi: 10.3390/pr11030940.
[23] A. Krupa, M. Lackowski, A. Jaworek, Capacitance sensor for measuring void fraction in small channels, *Measurement*, 2021, **175**, 109046, doi: 10.1016/j.measurement.2021.109046.
[24] A. Veisi, M. H. Shahsavari, G. H. Roshani, E. Eftekhari-Zadeh, E. Nazemi, Experimental study of void fraction measurement using a capacitance-based sensor and ANN in two-phase annular regimes for different fluids, *Axioms*, 2023, **12**, 66, doi: 10.3390/axioms12010066.
[25] A. M. Iliyasu, M. H. Shahsavari, A. S. Benselama, E. Nazemi, A. S. Salama, An optimised and novel capacitance-based sensor design for measuring void fraction in gas–oil two-phase flow systems, *Nondestructive Testing and Evaluation*, 2024, **39**, 2450-2466, doi: 10.1080/10589759.2023.2301492.
[26] A. Jaworek, A. Krupa, Gas/liquid ratio measurements by rf resonance capacitance sensor, *Sensors and Actuators A: Physical*, 2004, **113**, 133-139, doi: 10.1016/j.sna.2004.02.006.
[27] L. Zhai, R. Liu, H. Zhang, N. Jin, Complex admittance detection of horizontal oil-water two-phase flows using a capacitance sensor, *IEEE Sensors Journal*, 2019, **19**, 7489-7498, doi: 10.1109/JSEN.2019.2914312.
[28] A. A. Kendoush, Z. A. Sarkis, Improving the accuracy of the capacitance method for void fraction measurement, *Experimental Thermal and Fluid Science*, 1995, **11**, 321-326, doi: 10.1016/0894-1777(95)00035-6.
[29] S. M. Salehi, H. Karimi, A. A. Dastranj, R. Moosavi, Twin rectangular fork-like capacitance sensor to flow regime identification in horizontal co-current gas–liquid two-phase flow, *IEEE Sensors Journal*, 2017, **17**, 4834-4842, doi: 10.1109/JSEN.2017.2708663.
[30] R. Romero-Mendez, E. Berjano, Differences in the electric field distribution predicted with a mathematical model of cylindrical electrodes of finite length *vs*. infinite length: a comparison based on analytical solution, *Mathematics*, 2023, **11**, 4447, doi: 10.3390/math11214447.
[31] A. Dr. Uma Devi, K. Naveen Raj, M. Mugilan, S. L. Ananthan, S. N. Neha, T. Sutharsan, AI in healthcare, *International Research Journal on Advanced Engineering and Management (IRJAEM)*, 2025, **3**, 1100-1111, doi: 10.47392/irjaem.2025.0180.
[32] K. Daneshvar, M. J. Moradi, H. Hajiloo, A machine learning approach for predicting a full load-deflection behaviour of strengthened beams using fabric-reinforced cementitious matrix (FRCM), *Engineering Structures*, 2025, **337**, 120580, doi: 10.1016/j.engstruct.2025.120580.
[33] Sordo, Zineb, Eric Chagnon, and Daniela Ushizima. A Review on Generative AI For Text-To-Image and Image-To-Image Generation and Implications To Scientific Images, *arXiv preprint arXiv:2502.21151*, 2025, doi: 10.48550/arXiv.2502.21151.